Impact of Earthquake Types and Aftershocks on Loss Assessment of Non-Code Conforming Buildings: Case Study with Victoria, British Columbia

Solomon Tesfamariam[a)], M.EERI and Katsuichiro Goda[b)]

This paper presents a study on the impact of earthquake types (shallow crustal, deep inslab, and mega-thrust Cascadia interface earthquakes) and aftershocks on loss assessment of non-code conforming reinforced concrete (RC) buildings. The loss assessment is formulated within the performance-based earthquake engineering framework. The dependency between the maximum and residual interstory drift ratios are captured using copulas. Finite-element models that take into account key hysteretic characteristics of non-ductile RC frames were adopted and incremental dynamic analysis is utilized to compute collapse risk. The proposed procedure is applied to a set of 2-, 4-, 8- and 12-story non-ductile reinforced concrete frames located in Victoria, British Columbia, Canada. From the results, the aftershock showed marked difference for the 2-story building. At annual probability of 10^{-2} – 10^{-3}, crustal and in-slab events with M_w6.5 to M_w7.5 contributed the most to the loss as these events occur more frequently. At rarer annual probability of 10^{-3} – 10^{-4}, the Cascadia event having M_w8.5 to M_w9.0 is predominant and contributed the most to the loss.

INTRODUCTION

Southwestern British Columbia (BC) is an active seismic region, affected by complex regional seismicity (Hyndman and Rogers 2010). Three earthquake types, namely shallow crustal, deep inslab, and mega-thrust Cascadia interface earthquakes, contribute significantly to overall seismic hazard (Atkinson and Goda 2011; Figure 1). The crustal earthquakes occur in the upper crust of the continental plate and expected earthquake magnitudes of this kind are the moment magnitude M_w6.5 to M_w7.5. On the other hand, interface and inslab earthquakes occur at the plate boundary and inside the subducting slabs (i.e. ocean areas). Therefore, the

[a)] The University of British Columbia, Okanagan Campus, 3333 University Way, Kelowna, British Columbia, Canada V1V 1V7
[b)] University of Bristol, Queen's Building, University Walk, Bristol, United Kingdom BS8 1TR

source-to-site distances for the interface and inslab events are greater than those for the crustal earthquakes. The earthquake magnitude of the mega-thrust subduction earthquakes are typically M_w8 and above. Since 1900, destructive earthquakes have occurred: the 1918 and 1946 shallow crustal earthquakes in Vancouver Island, Canada and the 1949, 1965, and 2001 (Nisqually) deep inslab earthquakes in Washington, USA. Moreover, paleoseismic data, such as onshore tsunami deposits and submarine turbidite deposits (Goldfinger et al. 2008), indicate that mega-thrust earthquakes had occurred repeatedly in the Cascadia subduction zone, involving the oceanic Juan de Fuca, Gorda, and Explorer plates moving against the continental North American plate. Because of different source and path characteristics of these earthquakes, amplitude, duration, and frequency content of typical ground motions for the three types differ.

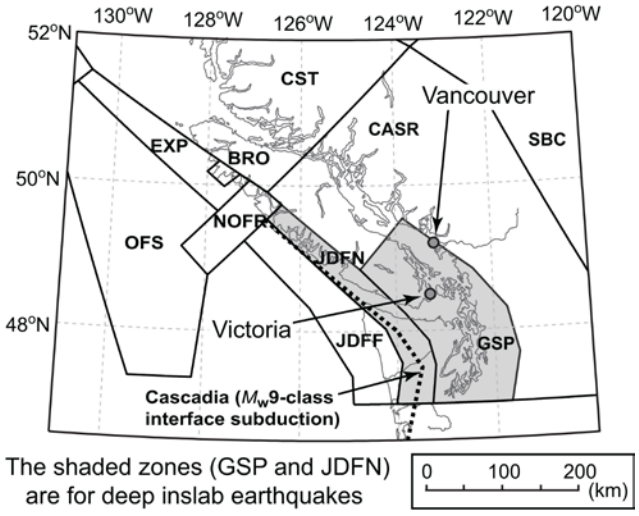

Figure 1. Seismic source zones in southwestern BC, Canada

A previous regional seismic risk assessment in Victoria, BC showed that older construction buildings are in high risk (Onur et al. 2005). Regional economic loss associated with a hypothetical M_w9 Cascadia earthquake scenario for BC can be significant (AIR Worldwide 2013). An accurate assessment of potential impact of future destructive earthquakes is essential for effective disaster risk reduction and requires decision-support tools that facilitate the quantitative seismic loss estimation (Goda et al. 2011; Ebrahimian et al. 2014). The problem can be further compounded by increasing intensity and frequency of observed aftershocks (e.g. 2011 M_w9.0 Tohoku earthquake in Japan, Goda et al. 2013; 2015 M_w7.8 Gorkha Nepal earthquake, Goda et al. 2015). As the three earthquake types in BC are prevalent, prudent record selection is also crucial to produce unbiased estimates of seismic vulnerability.

Koduru and Haukaas (2010) and Mahsuli and Haukaas (2013) have carried out loss assessment for Vancouver, BC with consideration of the three earthquake types. Koduru and Haukaas (2010) showed that for high-rise reinforced concrete (RC) buildings, crustal and subcrustal earthquakes contribute the most to the monetary loss. Mahsuli and Haukaas (2013) have showed that for spatially distributed buildings, subduction earthquake contribute the most to the prevalent loss. In the above two studies, the ground motions are generated through a stochastic model and did not consider mainshock and aftershock (MS-AS) sequences. Raghunandan et al. (2015) reported collapse risk assessment of older and newer RC buildings located in the Pacific Northwest subject to subduction and crustal earthquakes. Their study showed that subduction earthquakes contributed to the majority of the collapse risk. Their Pacific Northwest study did not include MS-AS sequences and loss assessment. Goda and Taylor (2012) have reported the effect of aftershocks from shallow crustal earthquakes on peak ductility demand. Goda et al. (2011) developed a probabilistic seismic loss model for a portfolio of existing wooden buildings in Vancouver subjected to the three earthquake types. Salami and Goda (2014) extended the seismic vulnerability models for wooden buildings by considering the aftershock effects in addition to major mainshocks. The above analyses are carried out only for 2-story timber structures. Tesfamariam et al. (2015) carried out seismic vulnerability assessment on a 6-story RC frame with unreinforced masonry infill due to MS-AS sequences. Their study did not consider loss assessment and the contribution of the three earthquake types were not delineated.

The major consideration in modeling seismic loss is the proper treatment of uncertainties in the quantification of demand and capacity, and cost incurred due to unsatisfactory performance. The uncertainty in demand, capacity, and ensuing damage can be quantified probabilistically through inelastic seismic demand prediction models, seismic fragility models, and damage-loss functions. For this purpose, the performance-based earthquake engineering (PBEE) methodology can be employed to assess seismic vulnerability of facilities and components that contribute to specified levels of consequences (Cornell and Krawinkler 2000). Three engineering demand parameters (*EDPs*) are considered in the loss assessment: maximum interstory drift ratio (MaxISDR), residual interstory drift ratio (ResISDR), and peak floor acceleration (PFA). The damage-loss analysis in this paper is carried out following a story-based loss estimation procedure proposed by Ramirez and Miranda (2009). Goda and Tesfamariam (2015) extended this model by developing a multivariate seismic demand model, where detailed characterizations of marginal probability distributions and dependence (copula) models of MaxISDR and ResISDR are considered. Tesfamariam and Goda (2015)

carried out a seismic loss assessment with a mega-thrust M_w9-class subduction earthquakes for a non-code conforming 4-story RC building in Victoria, BC. Goda and Tesfamariam (2016) extended this study to highlight implication of the loss assessment for seismic risk management decision making. The three earthquake types, however, have different duration and frequency content, and a comprehensive loss assessment study with consideration of MS-AS and varying building height is warranted for risk assessment and management decision actions. This paper extends the multi-variate loss assessment reported in Tesfamariam and Goda (2015) with consideration of varying building heights, 2-, 8-, and 12-story and with the seismicity of Victoria. The reported study accounts for:

- Consideration of probabilistic seismic hazard analysis (PSHA) for Victoria. The key features of the critical earthquake scenarios for a given location can be evaluated quantitatively via PSHA. Atkinson and Goda (2011) conducted seismic hazard studies for southwestern BC by incorporating recent advancements in seismology. Typical outputs from PSHA that are essential for seismic performance assessment of buildings and infrastructure are the uniform hazard spectra (UHS) and seismic deaggregation. The deaggredated loss assessment is provided for the three earthquake types.
- Earthquake types (shallow crustal earthquakes, deep inslab earthquakes, and mega-thrust Cascadia subduction earthquakes) by selecting applicable records for subduction environments from extensive ground motion datasets (including the 2011 Tohoku earthquake records which can be regarded as closest proxy for the Cascadia subduction events). For all building heights, impact of the earthquake types on the loss assessment is quantified.
- Mainshock-aftershock (MS-AS) sequences as earthquake excitation, and
- Multi-variate seismic demand modeling, focusing on MaxISDR and ResISDR, and PFA.

A computational flow of the PBEE utilized in this paper is illustrated in Figure 2. It consists of five basic steps. *First*, finite element (FE) models of the 2-, 4-, 8-, and 12-story RC frame are prepared to consider nonlinear behavior of elements. In the *second* step, through PSHA, the UHS for Victoria is generated. In the *third* step, a suite of ground motions which corresponds to a target seismic hazard level is selected on the basis of fundamental period of the structure (T_1). Multiple CMS for different earthquake types are employed as target response spectra (Baker 2011; Goda and Atkinson 2011). Each ground motion consists of mainshock and aftershocks (MS-AS). In the *fourth* step, the RC frames are analyzed for the

suite of MS-AS sequences and the performance parameters of interest are recorded for each motion, MaxISDR, ResISDR and PFA. In the *last* step, the story-based loss estimation is undertaken.

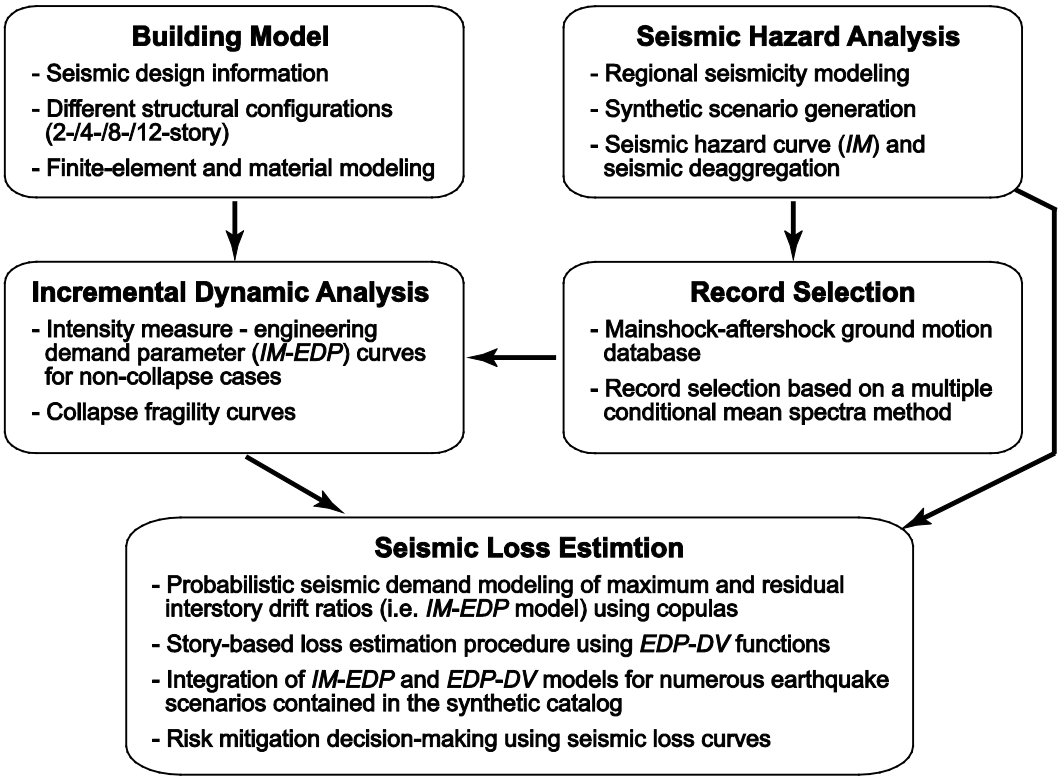

Figure 2. Probabilistic seismic loss estimation procedure.

STRUCTURAL MODEL

Tesfamariam and Goda (2015) studied the effect of MS-AS earthquake records on the loss assessment of a 4-story non-code conforming RC structure. This study extends the investigation to 2-, 8-, and 12-story non-code conforming RC buildings reported in Liel and Deierlein (2008). The buildings were designed as a space frame, according to the 1967 Uniform Building Code (UBC) seismic provisions (ICBO 1967). The design is governed by strength and stiffness requirements, as the 1967 UBC had few requirements for special seismic design or ductile detailing. Beam and column elements have the same amount of over-strength; each element is 15% stronger than the code-minimum design level.

The non-ductile structures are modeled in OpenSees using a lumped plasticity approach (Figure 3a). The lumped plasticity element models used to simulate plastic hinges in beam-column elements utilize a nonlinear spring model (Figure 3b). These finite-element models are capable of capturing important modes of deterioration that lead to side-sway collapse of RC frames (Haselton et al. 2008). Using modal analysis of the finite-element models, periods

of the first three modes are computed and summarized in Table 1. For comparison, results of the 4-storey building are incorporated in this paper.

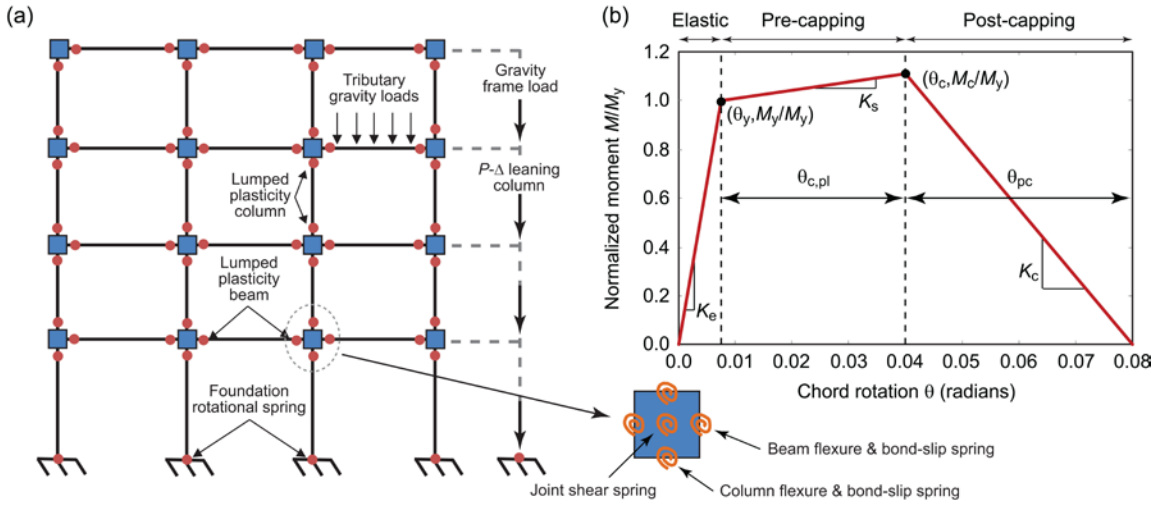

Figure 3. (a) Nonlinear finite-element model of a 4-story non-ductile RC frame and (b) backbone curve of an element model used for beam-column elements.

Table 1: First three fundamental periods of 2-, 4-, 8-, and 12-story RC frame buildings.

Building story	Period (s)		
	Mode-1	Mode-2	Mode-3
2	1.10	0.20	0.03
4	1.92	0.55	0.27
8	2.23	0.80	0.41
12	2.35	0.85	0.47

SEISMIC HAZARD AND INPUT GROUND MOTION SELECTION

The UHS at 2% probability of exceedance (PE) in 50 years is adopted as the basis for seismic design provisions for new construction in Canada. The seismic deaggregation identifies critical earthquake scenarios (for instance, in terms of magnitude, distance, and earthquake type) for a selected probability level. Figure 4a (and Figure 4b) shows a UHS at 2% PE in 50 years (black curve) for Victoria, where the site condition is set to site class C, which is represented by the average shear-wave velocity in the upper 30 m between 360 m/s and 760 m/s. Figures 4c and 4d show the seismic deaggregation results for T = 1.0 s and 2.0 s for 2% PE in 50 years. The selected vibration periods correspond to the adopted intensity measure (*IM*) for the 2-story building and the 4-, 8-, and 12-story buildings, respectively. T = 1.0 s is relatively close to the fundamental vibration period of the 2-story RC frame, while T = 2.0 s falls within the vibration periods of the 4-story to 12-story RC frames (Table 1). The vibration periods of *IM* are selected based on several factors and constrains, such as computability of seismic hazard values and consistency with the Canadian seismic hazard maps. In Figures 4c

and 4d, relative contributions due to crustal, mega-thrust (Cascadia) interface, and deep inslab earthquakes are indicated. The seismic deaggregation results suggest that seismic hazard values for longer vibration periods are affected more significantly by the large subduction events. The variable characteristics of the dominant scenarios are important for seismic performance evaluations and thus should be taken into account in selecting ground motion records for nonlinear dynamic analyses.

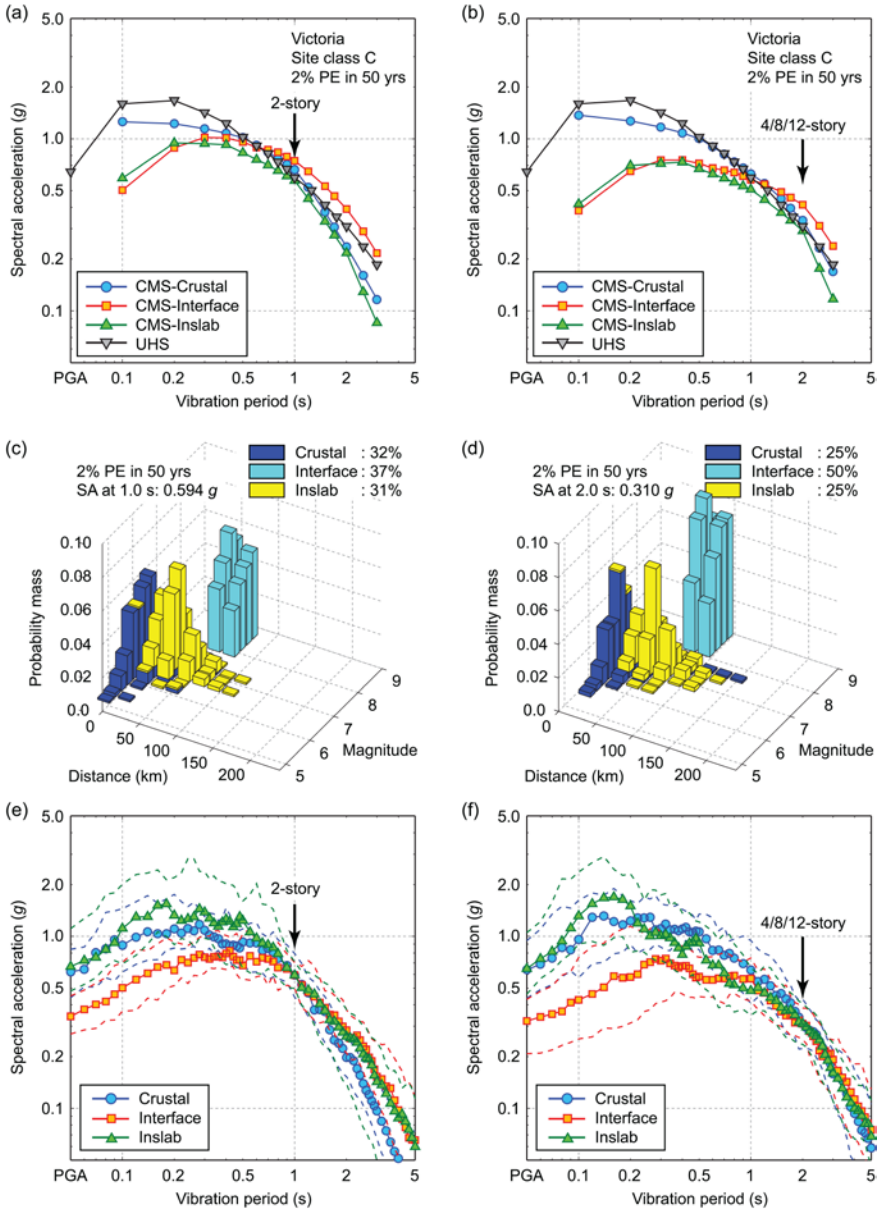

Figure 4. (a) Conditional mean spectra for T = 1.0 s for 2% PE in 50 years, (b) conditional mean spectra for T = 2.0 s for 2% PE in 50 years, (c) seismic deaggregation for T = 1.0 s and 2% PE in 50 years, (d) seismic deaggregation for T = 2.0 s and 2% PE in 50 years, (e) scaled response spectra of the selected ground motion records for T = 1.0 s and 2% PE in 50 years, and (f) scaled response spectra of the selected ground motion records for T = 2.0 s and 2% PE in 50 years. In (e) and (f), solid lines with markers correspond to median, while broken lines correspond to 16th and 84th percentiles.

Careful record selection is crucial to produce unbiased estimates of seismic vulnerability. In particular, when record scaling is implemented to reach high seismic excitation levels, record selection needs to account for the spectral shape effects (Luco and Bazzurro 2007). One practical method that is widely adopted for mitigating the record scaling bias is the conditional mean spectrum (CMS) method (Baker 2011). In the CMS-based record selection, the target response spectrum is modified based on dominant earthquake scenarios and relevant ground motion prediction equations at a selected probability level. Typically, the base target response spectrum for record selection is a UHS and is further modified based on the mean scenarios obtained from seismic deaggregation; several tens of ground motion records that match the modified target response spectrum (i.e. CMS) are selected as input motion. However, for the seismic environments in southwestern BC, it may be too simplistic to use a single target response spectrum because three dominant earthquakes with different characteristics are present (Figures 4c and 4d). For this reason, the multiple CMS-based record selection method proposed by Goda and Atkinson (2011) is adopted, which defines three different target spectra considering the different earthquake characteristics and ground motion prediction models for these earthquake types. Examples of the CMS for crustal, interface, and inslab earthquakes are shown in Figure 4a (for the 2-story building) and Figure 4b (for the 4-, 8-, and 12-story buildings). It is noted that the CMS for the interface events have richer spectral content with respect to other two earthquake types because of larger earthquake magnitudes and longer propagation paths.

A new composite database of real MS-AS sequences is compiled by combining the database that was constructed based on the Next Generation Attenuation database (Goda and Taylor 2012) and the new database for Japanese earthquakes from the K-NET, KiK-net, and SK-net (Goda et al. 2015). It is noteworthy that the new Japanese database includes records from the 2011 Tohoku earthquake, which may be considered as appropriate surrogate for the Cascadia subduction events. The composite dataset consists of 606 real MS-AS sequence records; 75 sequences are from the NGA database and 531 sequences are from the Japanese database (each sequence has two horizontal components). This database is the largest dataset for as-recorded MS-AS sequences and is sufficient to select a suitable set of record sequences by taking into account various requirements, such as earthquake type, magnitude, distance, and site class.

The record selection for the 2-story building and the 4-, 8-, and 12-story buildings is conducted by considering the multiple CMS specific to earthquake types, which are shown in

Figures 4a and 4b, respectively. The response spectrum of the candidate mainshock record (of an MS-AS sequence) is compared with the target CMS in a least square sense, and the 50 best matching mainshock records are accepted (note: each record/sequence consists of two horizontal components). The vibration period ranges considered for the response spectral matching are from 0.1 s to 2.5 s for the 2-story building and from 0.3 s to 3.0 s for the 4-, 8-, and 12-story buildings. The period ranges cover the two/three dominant vibration modes of the structural models (Table 1). To avoid excessive scaling of records, records that require scaling factors of more than 5.0 or less than 0.2 are excluded. The site conditions of the selected records are site class C or D (i.e. average shear-wave velocity ranges from 180 m/s to 760 m/s). It was necessary to relax the requirement for the soil condition of the candidate records with respect to the PSHA calculations. Nevertheless, using the target CMS for the site class C partially ensures that the selected records have response spectra shapes that are expected for site class C. In selecting the records, relative contributions of the three earthquake types are taken into account based on seismic deaggregation results (Figures 4c and 4d). For instance, the 50 MS-AS records that are chosen for the 2-story building consists of 16 crustal, 19 interface, and 15 inslab records (see Figure 4c). Another important assumption that is considered in our record selection is that large subduction records in Japan (i.e. M_w8.3 2003 Tokachi-oki earthquake and M_w9.0 2011 Tohoku earthquake) can be substituted for megathrust interface records in the Cascadia subduction zone. Although seismotectonic details of the two regions are different (and thus further research is needed), the current knowledge on the expected ground motions from the Cascadia subduction zone (only in terms of response spectra, not earthquake rupture processes) is reflected in the record selection because the target CMS for the interface earthquakes are derived from the regional PSHA study (Atkinson and Goda 2011). Figures 4e and 4f show scaled response spectra of the selected ground motion records for T = 1.0 s and 2.0 s, respectively. It can be observed that the long-period spectral content of the interface and inslab records for T = 1.0 s is greater than that of the crustal records, whereas such differences are not particularly noticeable for T = 2.0 s. The record information of the selected MS-AS sequences for the four buildings is provided in the electronic supplement to this paper.

To investigate the record characteristics of the selected MS-AS sequences, Figure 5 shows the normalized response spectra of the selected mainshock and major aftershock records for three earthquake types and for the 2-story building and the 4-, 8-, and 12-story buildings. For a given selected record sequence, response spectra of the mainshock and major aftershock (having the second largest magnitude within the sequence) are normalized by the peak ground

acceleration of the mainshock. Both median and 16/84th percentile curves are included in the figure. The normalized response spectral plots show the response spectral shapes of the mainshock records and the major aftershock records as well as their relative amplitudes of the aftershock records with respect to the mainshock records. Comparison of the response spectra of the mainshock records for three earthquake types indicates that the selected interface records contain richer long-period spectral content with respect to the other two earthquake types (consistent with the target CMS shown in Figures 4a and 4b). Moreover, relative amplitudes of the mainshock records and aftershock records depend on the earthquake types; on average, response spectra of the aftershocks for crustal earthquakes are significantly smaller than those of the mainshocks, while response spectra of the aftershocks for interface and inslab earthquakes are more similar to those of the mainshocks. Another important observation of the results shown in Figure 5 is that the variability of the aftershock response spectra is different for the three earthquake types; for instance, such variability for crustal earthquakes is greater than that for inslab earthquakes.

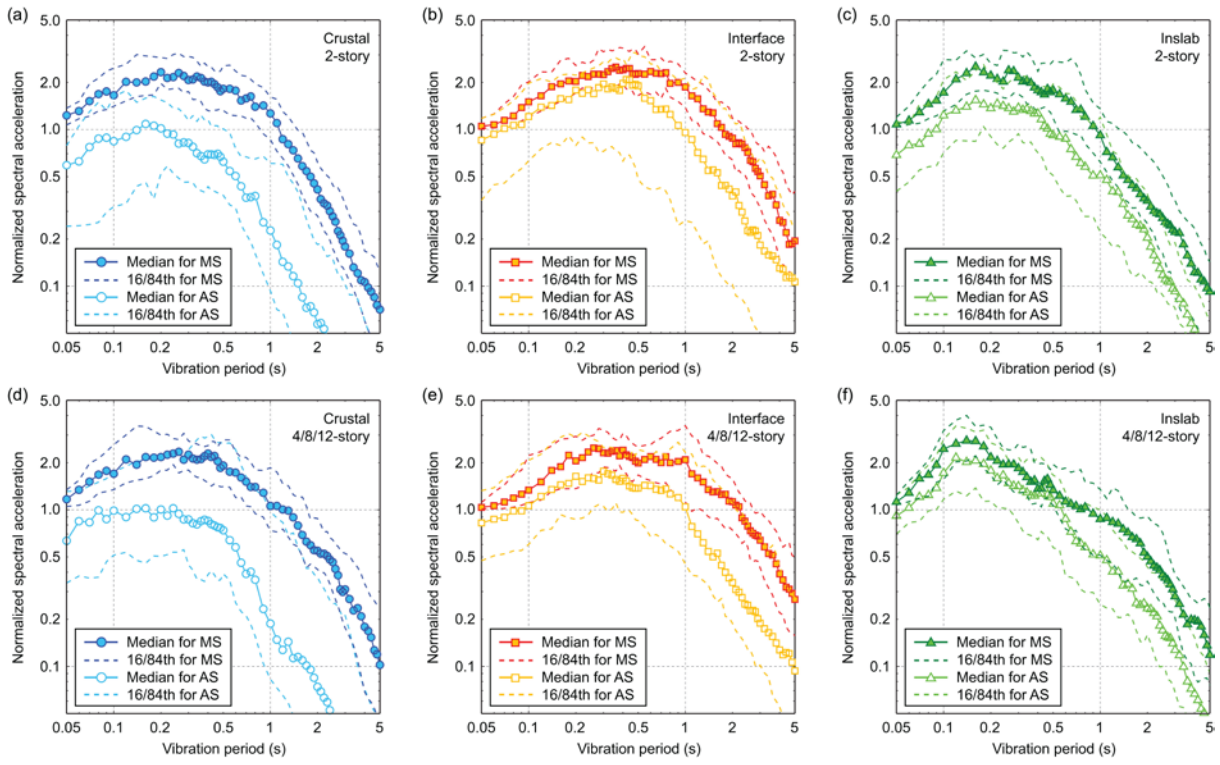

Figure 5. Normalized response spectra of the selected mainshock and major aftershock records: (a-c) crustal, interface, and inslab records for the 2-story building, and (d-f) crustal, interface, and inslab records for the 4-, 8-, and 12-story buildings. The response spectra of the records are normalized with respect to the peak ground acceleration of the mainshock records (this is applicable to the major aftershock records).

INCREMENTAL DYNAMIC ANALYSIS

Incremental dynamic analysis (IDA) implements a series of nonlinear dynamic analyses by scaling a set of input ground motions based on an adopted *IM*, and develops prediction equations of *EDP* (e.g. MaxISDR and ResISDR) at different *IM* levels. The *IM* selected in this paper is the spectral acceleration at the fundamental period $S_a(T_1)$ of a structure. For the different building story numbers, the maximum scaling required in IDA varies. For the 2-story building, the spectral acceleration at 1.0 s is selected as *IM* (Table 1) and the scaling range in IDA is varied from 0.05*g* to 1.4*g*. For the 4-, 8-, and 12-story buildings, the spectral acceleration at 2.0 s (i.e. *IM*) ranges from 0.05*g* to 0.7*g*. In general, numerical instability is encountered when the inter-story drift response of the frames exceeds 0.10. The first occurrence of such large deformation responses is treated as 'collapse' (Vamvatsikos and Cornell 2002). IDA is carried out for the 2-, 4-, 8-, and 12-story RC frames using the set of 50 MS records as well as a set of 50 MS-AS sequences, which are selected based on the multiple CMS-based procedure. The comparison of the *EDPs* obtained using the MS records and the MS-AS records allows quantifying the effects of aftershocks on the earthquake damage potential. When the MS-AS records are used as ground motion input, intermediate damage states of structures are reflected in the final *EDP* values that are obtained from the IDA. Due to the limitation of space, the results for PFA, which is also used as an *EDP* to calculate the seismic loss of a building (see Tesfamariam and Goda 2015), are not discussed in this study.

EFFECTS OF BUILDING HEIGHT AND MS-AS EARTHQUAKES

The IDA results for both MS records and MS-AS sequences (i.e. *EDP-IM* plot) are shown in Figure 6 (for MaxISDR) and Figure 7 (for ResISDR). The results are based on non-collapse structural responses. To present the uncertainty of the IDA results, 16^{th}-84^{th} percentile curves (corresponding to mean ± one standard deviation), are included in the figures. The overall characteristics of the IDA curves for MaxISDR and ResISDR are different. The former increases gradually with the seismic intensity level, while the latter increases rapidly when the seismic intensity level reaches in the range of 0.2-0.3*g* for the 2-story building and 0.15-0.20*g* for the 4-, 8-, and 12-story buildings. With lower intensity measures, the structure is undergoing linear deformation, i.e. MaxISDR response is linear. However, with increasing *IM*, the structure undergoes non-linear deformation with potential onset of permanent deformation. The permanent deformation is associated with ResISDR and this is the potential reason why it is prevalent with higher intensity *IM*. It is noteworthy that the uncertainty of ResISDR is much greater than that of MaxISDR, as noted by Ruiz-García and Miranda

(2006). Comparison of the IDA results for the 4-, 8-, and 12-story buildings, which adopt the same *IM*, shows that for a given seismic excitation level, both MaxISDR and ResISDR decrease with the story number; therefore, for the considered non-ductile RC frames the order with respect to higher vulnerability levels is: 4-story > 8-story > 12-story building.

The results shown in Figures 9 and 10 suggest that the earthquake event types have noticeable effects on the IDA results. For both MaxISDR and ResISDR, the median curves for interface events are severer than those for the crustal and inslab events; i.e. for a given *IM* level (vertical axis), greater *EDP* values (horizontal axis) are attained. The increased seismic demand potential for the interface records is related to the rich long-period spectral content and the long-duration excitation. The latter makes noticeable influence, especially for ResISDR, because the structure tends to oscillate within an inelastic domain for a longer time. Another observation is that the variability of the IDA curves for inslab records is significantly smaller than those for crustal and interface records. In short, physical features of ground motion records have influence on the seismic demand potential assessment.

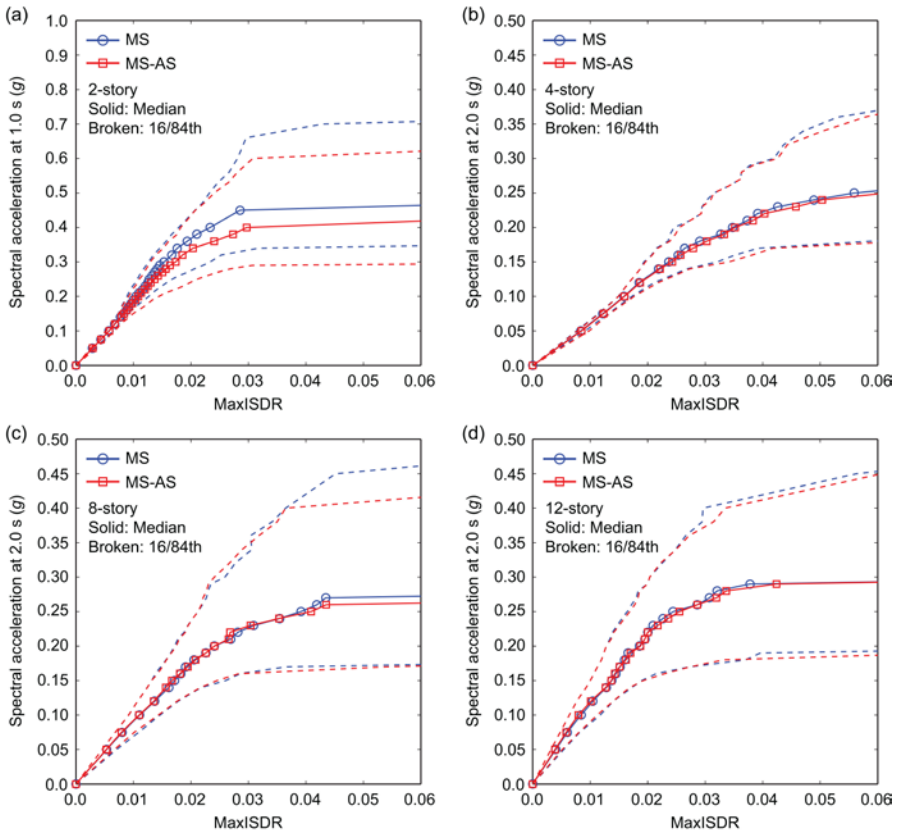

Figure 6. IDA results (MaxISDR) by considering MS and MS-AS records: (a) 2-story, (b) 4-story, (c) 8-story, and (d) 12-story.

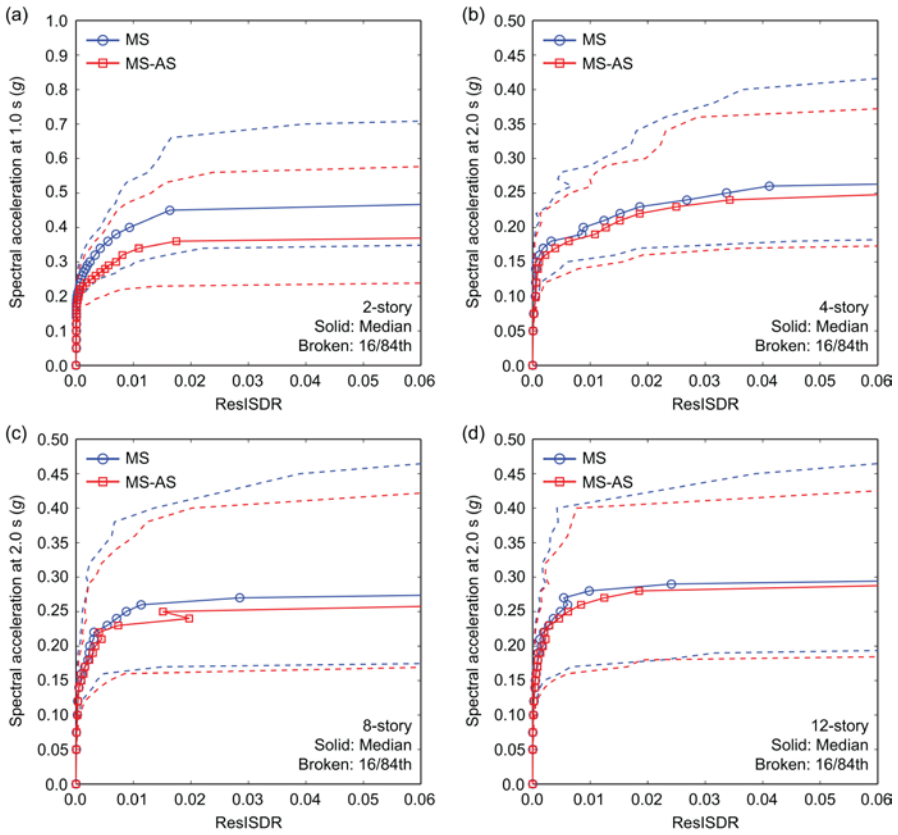

Figure 7. IDA results (ResISDR) by considering MS and MS-AS records: (a) 2-story, (b) 4-story, (c) 8-story, and (d) 12-story.

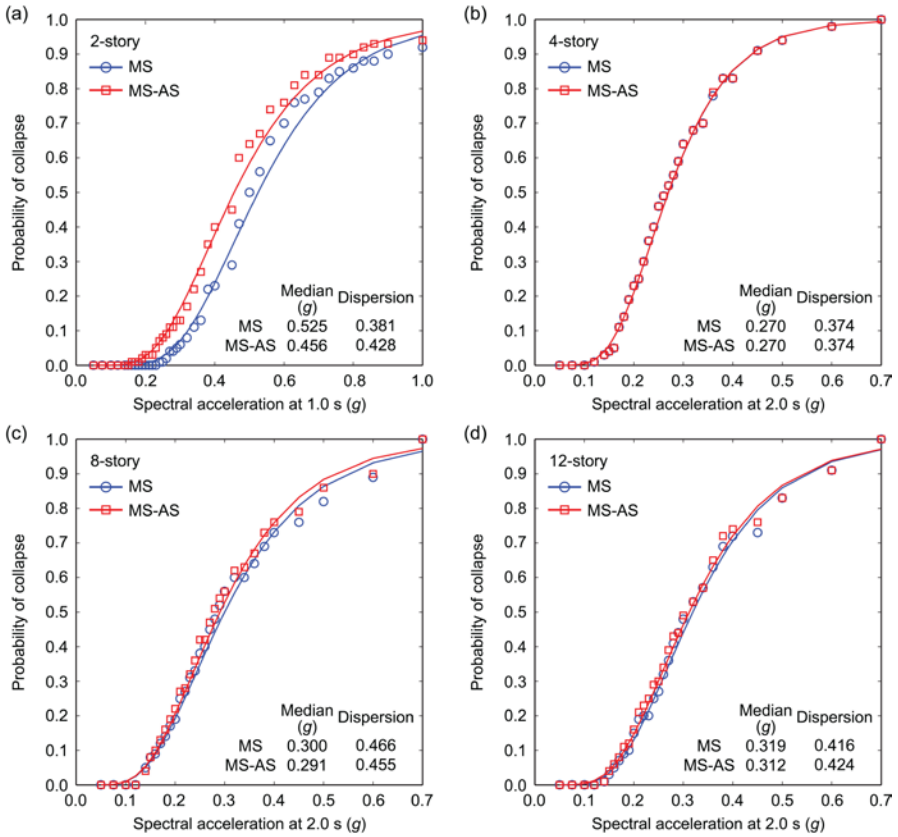

Figure 8. Collapse fragility results by considering MS and MS-AS records: (a) 2-story, (b) 4-story, (c) 8-story, and (d) 12-story.

Figure 8 shows the collapse fragility results (raw data and fitted lognormal curve; two lognormal model parameters, median and dispersion, are indicated) for MS records and MS-AS sequences. The impact of aftershocks is pronounced for the 2-story building, where the median collapse capacity is reduced by 13% (i.e. the curve is shifted towards left). On the other hand, the collapse fragility curves of the 4-, 8-, and 12-story buildings show no or slight differences. These results are consistent with the IDA curves shown in Figure 6. The clear contrast of the aftershock effects on the collapse fragility for the low-rise and mid-/high-rise buildings can be explained by the fundamental vibration periods of the structures and the dominant spectral content of the aftershock records. More specifically, by looking at Figure 5, it can be observed that the spectral content of the aftershock record decreases rapidly with the vibration period. When the fundamental vibration period of the structure is relatively short, spectral amplitudes of the aftershocks can be intense. The chance of such large spectral amplitudes becomes less when a long-period structure is considered. The decay of the spectral content of the aftershocks with respect to that of the mainshocks is influenced by various factors, and one of the key aspects is the earthquake magnitude (other factors include source mechanism and source-to-site distance). On average, the magnitude of major aftershocks is smaller than that of the mainshocks by about 1.0 to 1.2 unit (Goda and Taylor 2012; Goda et al. 2015). The comparison of collapse fragility results for the 4-, 8-, and 12-story buildings highlights that the median collapse capacity as well as the dispersion (i.e. slope of a fragility curve) tends to increase with the story number; the differences of the collapse fragility curves are more pronounced at the greater seismic excitation levels. For example, at $IM = 0.3g$, the corresponding probability of collapse for the 4-, 8-, and 12-story buildings are 0.61, 0.51, and 0.44, respectively. The decrease in vulnerability is as a result of increase in the prevalent first mode periods and being subject to lower *IM*s.

EFFECT OF EARTHQUAKE TYPES

The IDA results for different earthquake types are developed by considering MS-AS records and are shown in Figure 9 (for MaxISDR) and Figure 10 (for ResISDR); broken curves correspond to the mean ± one standard deviation. It is noted that the calculated confidence interval of the IDA results is less stable because the number of data points is less than the combined cases shown in Figures 6 and 7. Therefore, the results should be interpreted with caution.

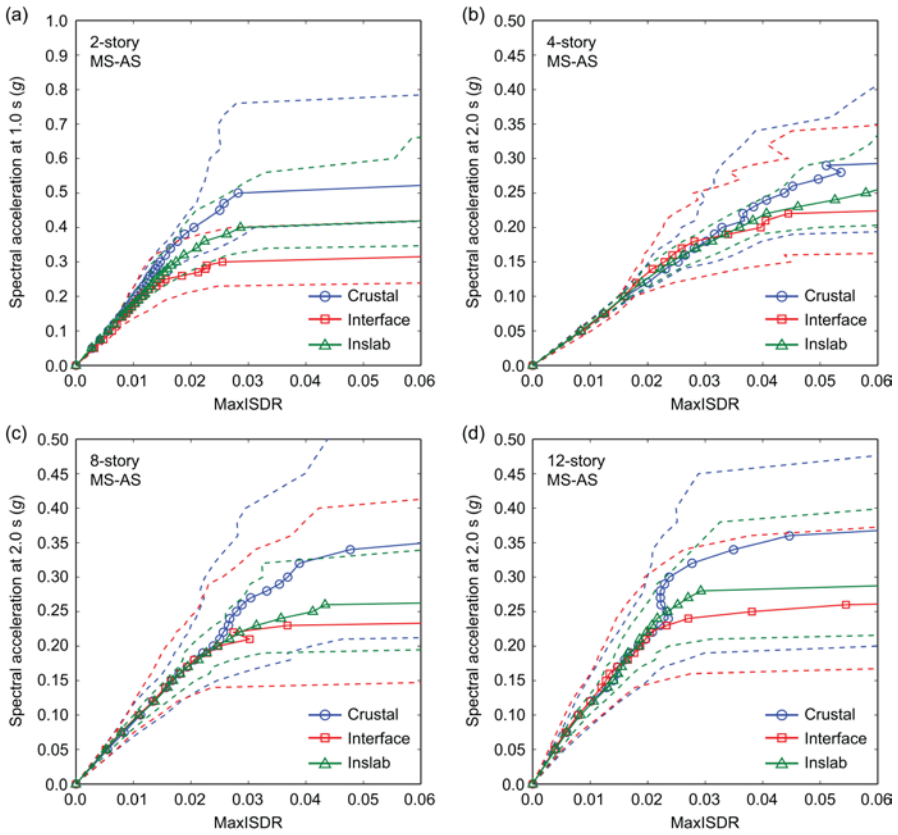

Figure 9. IDA results (MaxISDR) by considering MS-AS records and earthquake types: (a) 2-story, (b) 4-story, (c) 8-story, and (d) 12-story.

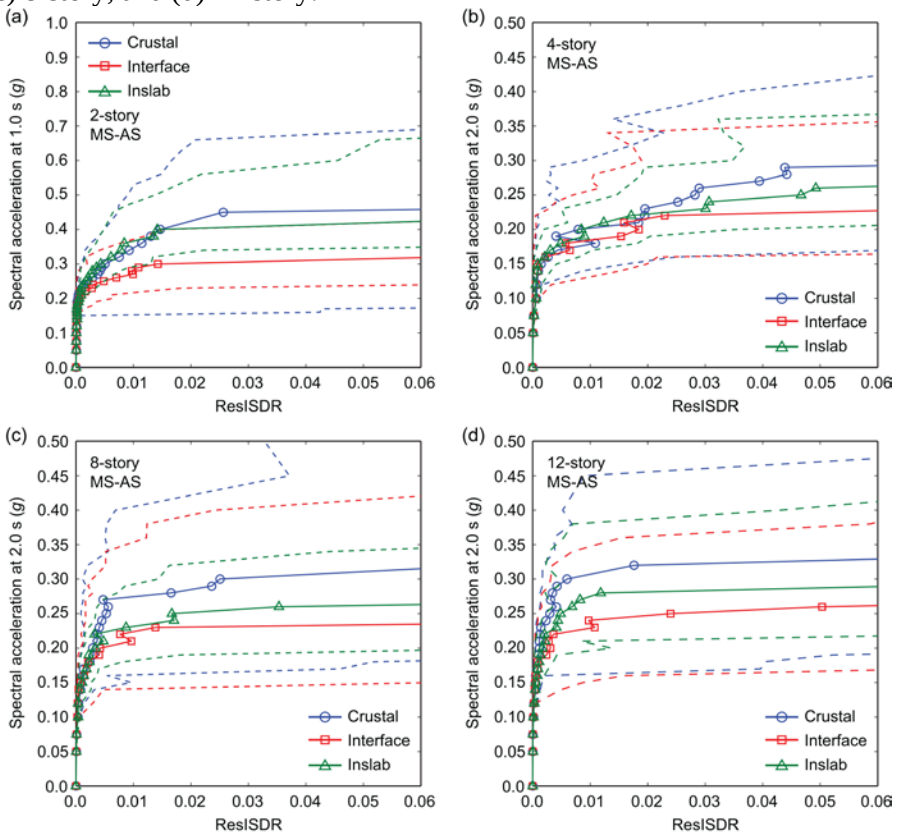

Figure 10. IDA results (ResISDR) by considering MS-AS records and earthquake types: (a) 2-story, (b) 4-story, (c) 8-story, and (d) 12-story.

A comparison of the collapse fragility curves for the three earthquake types is shown in Figure 11, when MS-AS sequences are used as seismic input. For the 2- and 4-story

buildings, the results indicate that the collapse potential due to the interface events is greater than that due to the inslab and crustal events. Similarly, for the 8- and 12-story buildings, the interface event is greater up to *IM* = 0.3-0.35*g*, and beyond this point, the inslab event is higher. The crossing of the fragility curves can be attributed to the small variability of the nonlinear structural responses due to the inslab records, in comparison with the crustal and interface records. This might be a genuine feature but can also be artificial because the number of the inslab records for the 8- and 12-story cases is smaller than that for the 2-story case. On the other hand, this does not apply to the crustal events, which have the similar number of record components that are used for deriving the IDA results. Overall, the results shown in Figure 11 confirm that ground motion characteristics of different earthquake types are important in characterizing both non-collapse and collapse seismic vulnerabilities of the RC frames.

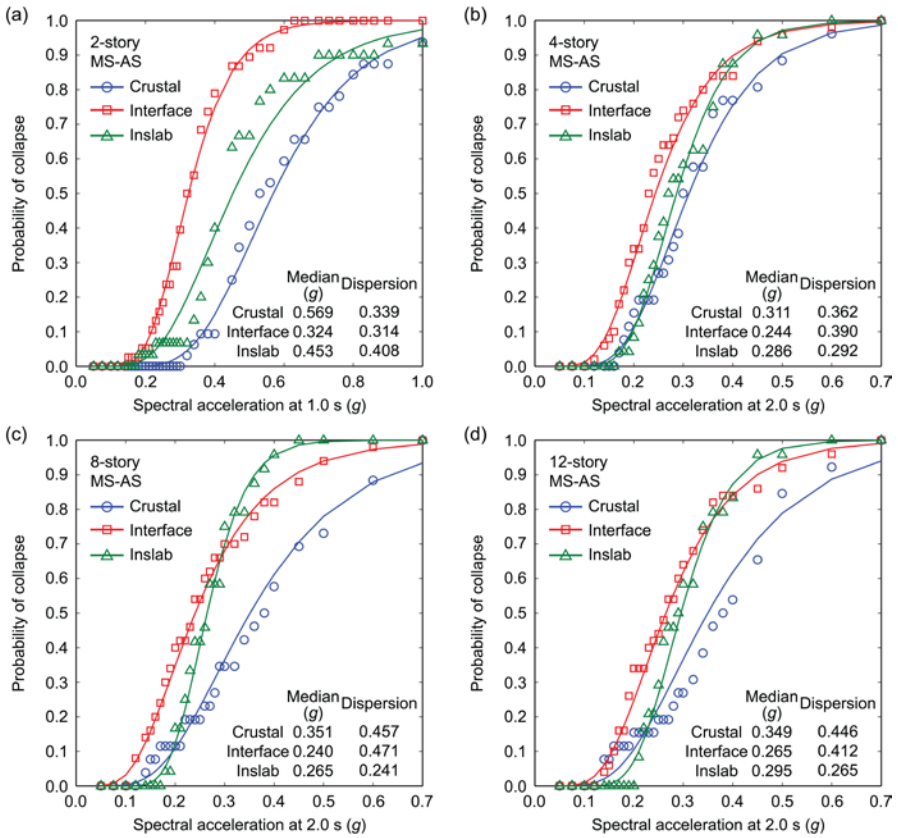

Figure 11. Collapse fragility results by considering MS-AS records and earthquake types: (a) 2-story, (b) 4-story, (c) 8-story and (d) 12-story.

COUPLA-BASED SEISMIC DEMAND MODELING

MaxISDR and ResISDR are statistically dependent (Goda and Tesfamariam 2015) and this should be taken into account when these *EDP*s are characterized. For the seismic demand modeling, first, marginal probability distributions of MaxISDR and ResISDR should be developed, and second, corresponding dependence needs to be characterized. The

probabilistic modeling of MaxISDR and ResISDR is performed at individual *IM* levels using non-collapse MaxISDR and ResISDR data (note: the number of available data points for seismic demand modeling decreases with the *IM* level because more data fall into collapse states).

Figure 12a shows the scatter plot for the 2-story building by considering MS-AS records at 5% PE in 50 years level. In the figure, marginal distributions of MaxISDR and ResISDR are plotted along the horizontal axis and vertical axis, respectively. It is noted that ResISDR has a heavy right tail. For MS records and MS-AS sequences, Goda and Tesfamariam (2015) showed that the Frechet distribution (Equation 1) and generalized Pareto distribution (Equation 2) are suitable for MaxISDR and ResISDR, respectively (note: the fitting performance of the lognormal distribution to MaxISDR is founded to be good). The probability density functions of the Frechet and the generalized Pareto models are given by:

$$f(x) = \frac{\xi}{\sigma}\left(\frac{x-\mu}{\sigma}\right)^{-1-\xi} \exp\left[-\left(\frac{x-\mu}{\sigma}\right)^{-\xi}\right], \text{ and} \quad [1]$$

$$f(x) = \frac{1}{\sigma}\left(1+\xi\frac{x-\mu}{\sigma}\right)^{-(1/\xi+1)} \quad [2]$$

where μ is the location parameter, σ is the scale parameter, and ξ is the shape parameter. These marginal distributions are non-normal (in particular, ResISDR); in such cases, conventional multi-variate normal (or lognormal) distribution modeling is not ideal, and a more elaborate approach is necessary.

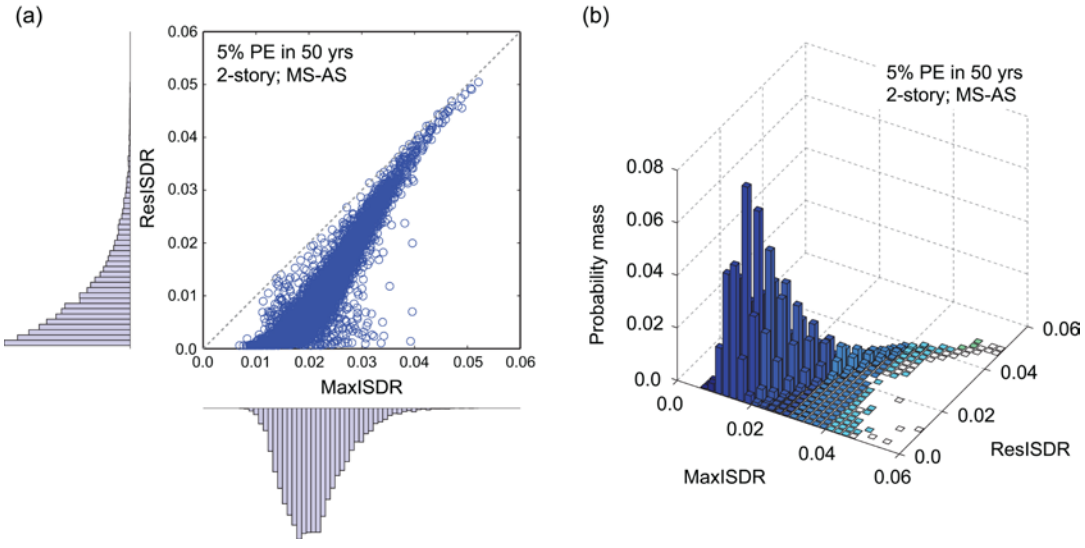

Figure 12. (a) Scatter plot and corresponding marginal probability distributions of MaxISDR and ResISDR and (b) joint distribution of MaxISDR and ResISDR for the 2-story building at 5% probability of exceedance in 50 years.

The dependence of MaxISDR and ResISDR can be characterized by using elliptical copulas, such as normal and *t*, and Archimedean copulas, such as Gumbel, Frank, and Clayton (McNeil et al. 2005). The asymmetric Archimedean copula is a mixture of an Archimedean copula and the independence copula; this copula class is useful for modeling data that exhibit uneven distribution of the data points along the upper-left-lower-right diagonal line in the transformed space. In the context of joint probability distribution modeling of MaxISDR and ResISDR, the uneven distribution of the data is related to the physical relationship between MaxISDR and ResISDR (i.e. MaxISDR ≥ ResISDR; Goda and Tesfamariam 2015). To model the observed dependence of MaxISDR and ResISDR (e.g. scatter plot shown in Figure 12a), parametric copula functions are fitted to empirical copula samples using the maximum likelihood method (McNeil et al. 2005). The copula fitting of MaxISDR and ResISDR at various *IM* levels suggests that overall, the Gumbel (or asymmetrical Gumbel) copula is suitable for the majority of the cases examined in this study.

The developed statistical seismic demand models of MaxISDR and ResISDR can be used for seismic performance evaluation of structures. For instance, considering the fitted dependence function for the 2-story building at 5% PE in 50 years, numerous copula samples are first generated; their marginal distributions are uniformly distributed with the specified dependence characteristics. Using the simulated copula samples and the fitted marginal distribution models for MaxISDR and ResISDR, pairs of MaxISDR and ResISDR samples can be obtained using the inverse transformation method. The results of 5,000,000 simulations are presented in Figure 12b. Indeed, similar figures can be generated for different building story numbers as well as seismic hazard levels. The copula-based seismic demand modeling outlined in this section will be used to develop seismic loss ratios based on *IM-DV* functions and to carry out loss assessment.

SEISMIC LOSS ESTIMATION

The formulation of the story-based seismic loss estimation simplifies a process of calculating seismic loss (i.e. *DV*) as a function of *EDP*, rather than *DM*, and it requires less information on structural details and their costs. The seismic loss L_T for given *EDP* can be expressed as (Ramirez and Miranda 2009):

$$L_T = L_{NC} + L_D + L_C \quad [5]$$

where L_{NC}, L_D, and L_C are the seismic losses for non-collapse repairs (*NC*), demolition (*D*), and collapse (*C*) cases, respectively. The three situations are disjoint and mutually exclusive.

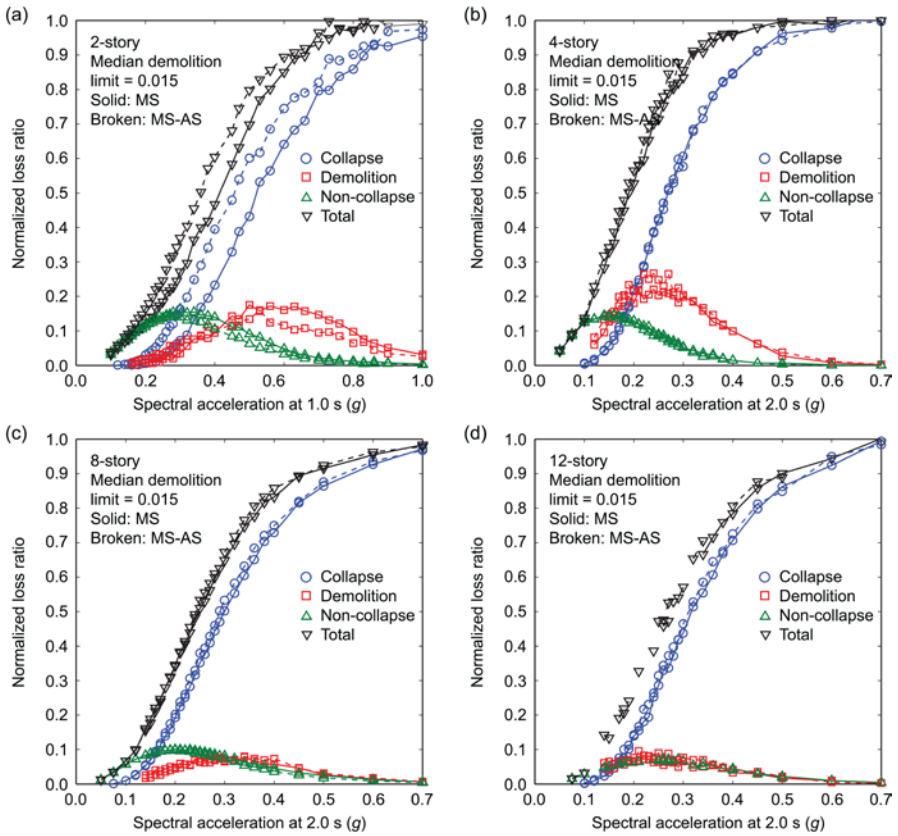

Figure 13. IM-DV functions for collapse, demolition, non-collapse damage, and total loss by considering the median demolition damage state limit of 0.015 and dispersion of 0.3: (a) 2-story, (b) 4-story, (c) 8-story, and (d) 12-story.

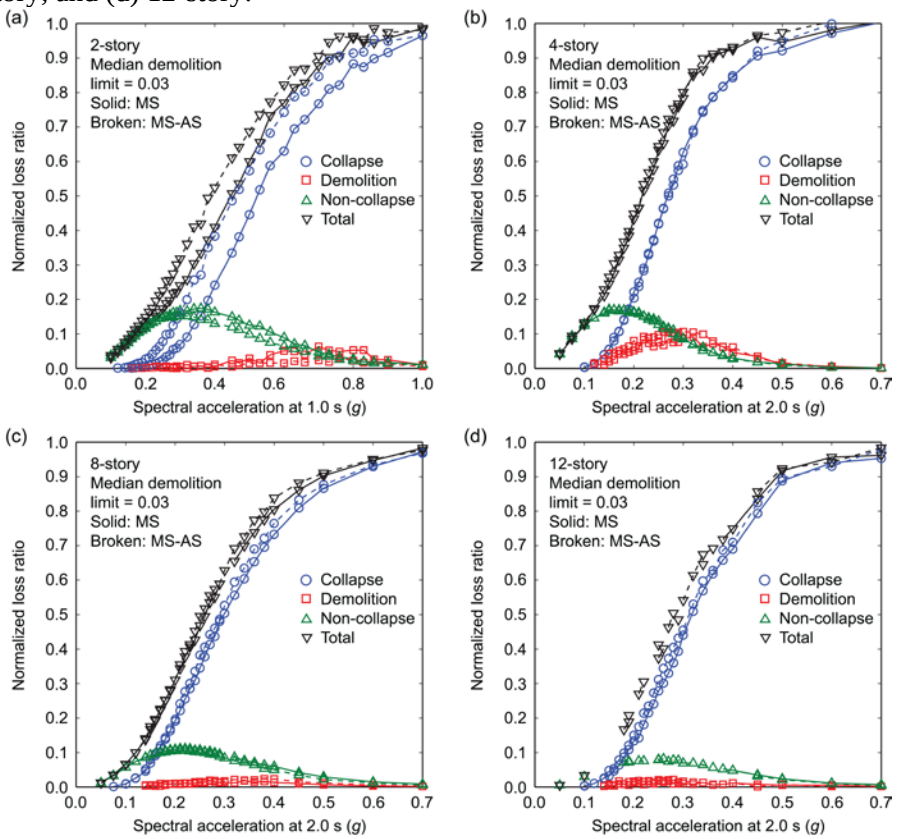

Figure 14. IM-DV functions for collapse, demolition, non-collapse damage, and total loss by considering the median demolition damage state limit of 0.03 and dispersion of 0.3: (a) 2-story, (b) 4-story, (c) 8-story, and (d) 12-story.

The numerical evaluation of L_T in probabilistic seismic risk analysis calculations is facilitated as follows: (i) collapse probability is assessed for *EDP*; if collapse is predicted, then $L_T = L_C$; (ii) demolition is considered for non-collapsed structure and it is determined according to a realized value of ResISDR (contained in *EDP*) in comparison with the lognormal limit state function for demolition, $G(D \mid \text{ResISDR}) = 1 - \Phi(\log(\text{ResISDR}/\mu_D)/\sigma_D)$ where Φ is the standard normal distribution function, and μ_D and σ_D are the median and logarithmic standard deviation (dispersion) of the demolition fragility curve, respectively; if demolition is predicted, then $L_T = L_D$; and (iii) otherwise, L_{NC} is assessed by using *EDP-DV* functions for non-collapse cases. It is noted that L_{NC}, L_D, and L_C are random variables.

For illustration, mean *IM-DV* functions are developed by generating 10,000 samples of normalized seismic loss ratios for each *IM* level. Figures 13 and 14 depict the *IM-DV* functions for *C*, *D*, *NC*, and total loss by considering the median demolition damage limit state parameters of 0.015 and 0.03, respectively. Results for both MS and MS-AS cases are included in the figures. Figures 13 and 14 show that, for all building heights, with increasing *IM*, the collapse damage normalized loss ratio increases, and the non-collapse damage and demolition damage loss ratio decreases. The results indicate the most likely loss generation modes for a given seismic excitation level and thus are useful for deciding seismic risk mitigation actions. As reflected with the IDA and collapse results, the effect of the aftershocks on the *IM-DV* functions for the 2-story building is significant. At *IM* = 0.4g for the 2-story and *IM* = 0.2g for the 4- to12-story buildings (which approximately correspond to the seismic hazard at the return period of 1000 years), for the case of the median demolition limit of 0.015 (Figure 13), the non-collapse damage consists of 10 to 15% with respect to the total replacement cost. On the other hand, the demolition-related damage consists of 10%, 20%, 5%, and 5% for the 2-, 4-, 8-, and 12-story buildings, respectively. The remaining parts of the loss percentages are due to collapse damage.

The procedure for developing the *EDP-DV* functions for the non-ductile RC frame follows the method suggested by Ramirez and Miranda (2009). First, component fragility groups (i.e. damage sensitivity) and story-based cost distributions are assigned to major building components. The damage sensitivities are based on structural and non-structural drift-sensitive components and non-structural acceleration components; typical proportions of the costs for drift-sensitive and acceleration-sensitive components are approximately 60% and 40%, respectively. The expected (normalized) loss in component *j* conditioned on *NC* and

EDP, $E[L_j|NC,EDP_j]$ is a function of the component's repair cost when it is in a different damage state and the probability of being in each damage state:

$$E\left[L_j \mid NC, EDP_j\right] = \sum_{i=1}^{m} E\left[L_j \mid NC, DS_i\right] p\left(DS = ds_i \mid NC, EDP_j\right) \quad [6]$$

where m is the number of damage states for component j, $E[L_j|NC,DS_i]$ is the expected value of the normalized loss for component j when it is in a damage state i, DS_i, and $p(DS=ds_i|NC,EDP_j)$ is the probability of the j^{th} component being in a damage state i, ds_i, given that it is subjected to a demand of EDP_j. The probability of being in each damage state for component j can be obtained from component-specific fragility functions. The *EDP-DV* functions are developed based subcontractor category (e.g. concrete, finish, and mechanical), in addition to story as well as damage sensitivity. The main reason for such development is to take into account uncertainties of damage-loss functions adequately, noting that probability distribution type (i.e. lognormal distribution) and variability (i.e. coefficient of variation) for the *EDP-DV* functions are available for subcontractor basis only. Further details on the seismic loss estimation can be found in Tesfamariam and Goda (2015).

Table 2: Four analysis cases for loss assessment.

Calculation cases	Demolition limit state parameter [μ_D, σ_D]	Additional uncertainty [collapse, non-collapse, *EDP-DV*]
Case 1	[0.015, 0.3]	[0.0, 0.0, 0.0]
Case 2	[0.03, 0.3]	[0.0, 0.0, 0.0]
Case 3	[0.015, 0.3]	[0.5, 0.25, 0.25]
Case 4	[0.03, 0.3]	[0.5, 0.25, 0.25]

To investigate the key issues related to the developed seismic loss estimation tool as well as the effects of aftershocks on the estimated seismic loss, four analysis cases are set up (Table 2). Specifically, for all building heights, the base case (Case 1) considers that: the demolition limit state parameters are [0.015, 0.3] and no additional sources of uncertainty (for collapse fragility, non-collapse vulnerability models, and *EDP-DV* functions) are taken into account. For the base case, the uncertainties associated with collapse and non-collapse damage and *EDP-DV* functions are determined based on the analytical evaluations of the *EDPs* and loss values, which may be considered to be the lower limit of such uncertainties. Cases 3 and 4 incorporate these uncertainties to investigate their impact on the loss assessment results.

For Case 1, seismic loss curves (i.e. plot of seismic loss as a function of annual probability) by considering MS-based and MS-AS-based seismic demand models with and without demolition in evaluating seismic loss, are obtained and shown in Figure 15. Cases 2

to 4 (Figures 16 to 18) show similar trend as shown in Figure 15. For probability of 4×10^{-4} (i.e. annual exceedance probability level in the National Building Code of Canada), the loss estimation results are summarized in Table 3. The results are presented as normalized loss with respect to the replacement costs of the buildings. From Figures 15 to 18 and Table 3, the key observations from the seismic loss estimation results are:

(i) Figure 15 (Case 1) investigates the effects of aftershocks when the median demolition limit state parameter is relatively low (= 0.015). The seismic loss curves in Figure 15 shows that the aftershocks have appreciable influence for the 2-story building (e.g. 12% increase in terms of annual mean loss), whereas their effects become smaller as the building story increases (e.g. 3-4% increase in terms of annual mean loss). The significant effects due to the aftershocks for the 2-story building are attributed to the increases of seismic demands, in particular ResISDR (Figures 7 and 8).

(ii) Figure 15 also shows that for the 2- and 4-story buildings, the consideration of the demolition failure modes increases the seismic loss curve noticeably because of large ResISDR. For example, at annual probability of 4×10^{-4}, with consideration of the demolition failure modes and MS earthquake, the seismic loss curves of the 2- and 4-story buildings increased by 10% and 23%, respectively (Table 3). The effect decreases for the 8-story that showed a difference of only 5%. For the 12-story, the effect is about 15%.

(iii) Figure 16 (Case 2) investigates the effects of aftershocks when the median demolition limit state parameter is relatively high (= 0.03). For the 2- and 4-story buildings, at 10^{-3} and lower probability levels, the effect of MS-AS sequences has increased the prevalent loss. For the 2- and 8-story buildings, the loss assessment difference between the demolition and no-demolition is small. At 10^{-4} probability levels, for the 4-story building, the increase was 11%.

(iv) Figures 17 and 18, respectively, show results for Cases 3 and 4 (note: the MS-AS (Demolition) case only). The results are to show the combined effects of the demolition damage limit state parameters and additional uncertainties for collapse fragility, non-collapse vulnerability models, and *EDP-DV* functions in the loss calculations. The increase owing to the model variations can be as large as 100% (depending on probability level and story height). At 10^{-4} probability levels, the increase was 15-20%. The shapes of the seismic loss curves are largely identical but are shifted upward, as compared with Figures 15 and 16, respectively.

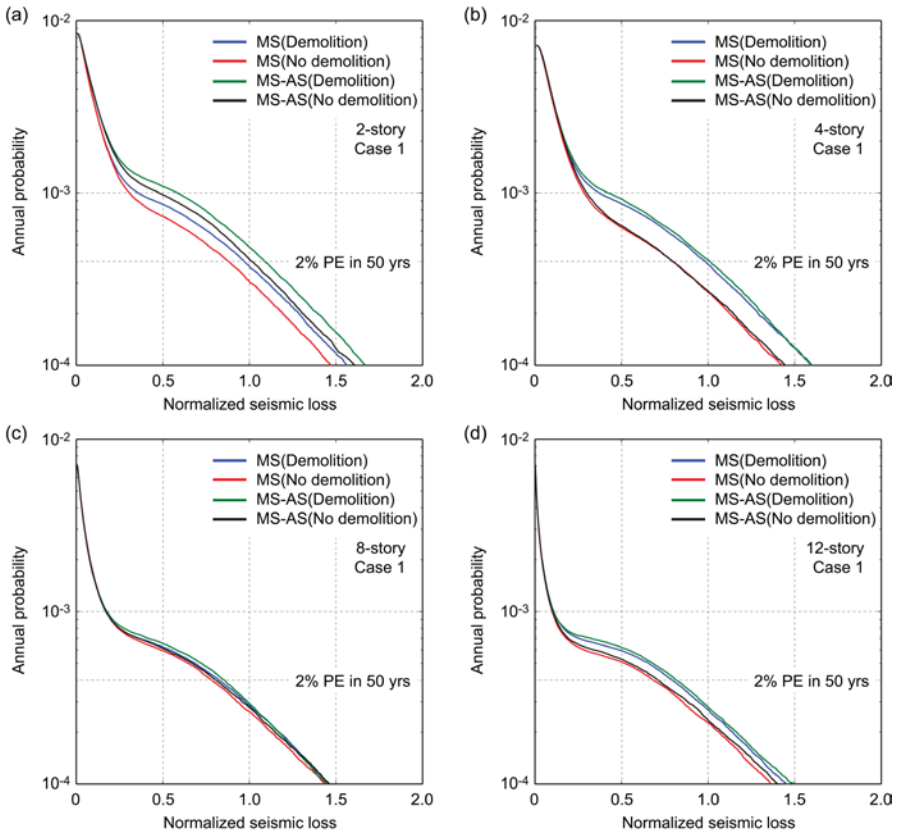

Figure 15. Seismic loss curves for MS records and MS-AS sequences with and without demolition failure cases (Case 1): (a) 2-story, (b) 4-story, (c) 8-story, and (d) 12-story.

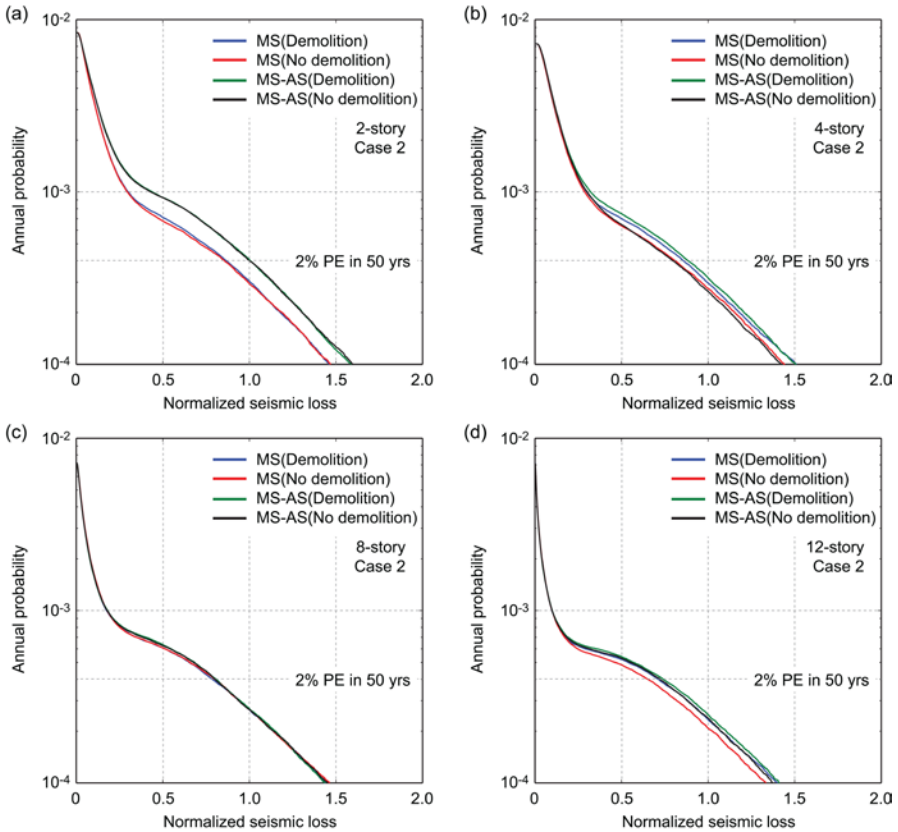

Figure 16. Seismic loss curves for MS records and MS-AS sequences with and without demolition failure cases (Case 2): (a) 2-story, (b) 4-story, (c) 8-story, and (d) 12-story.

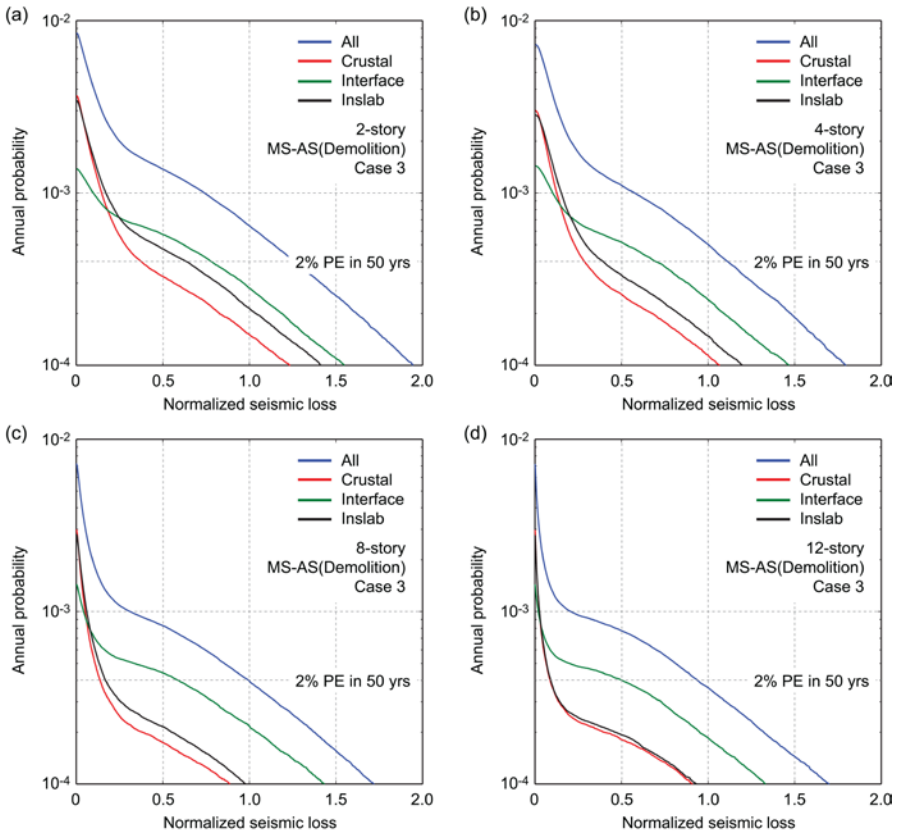

Figure 17. Seismic loss curves for MS-AS sequences and earthquake types (Case 3): (a) 2-story, (b) 4-story, (c) 8-story, and (d) 12-story.

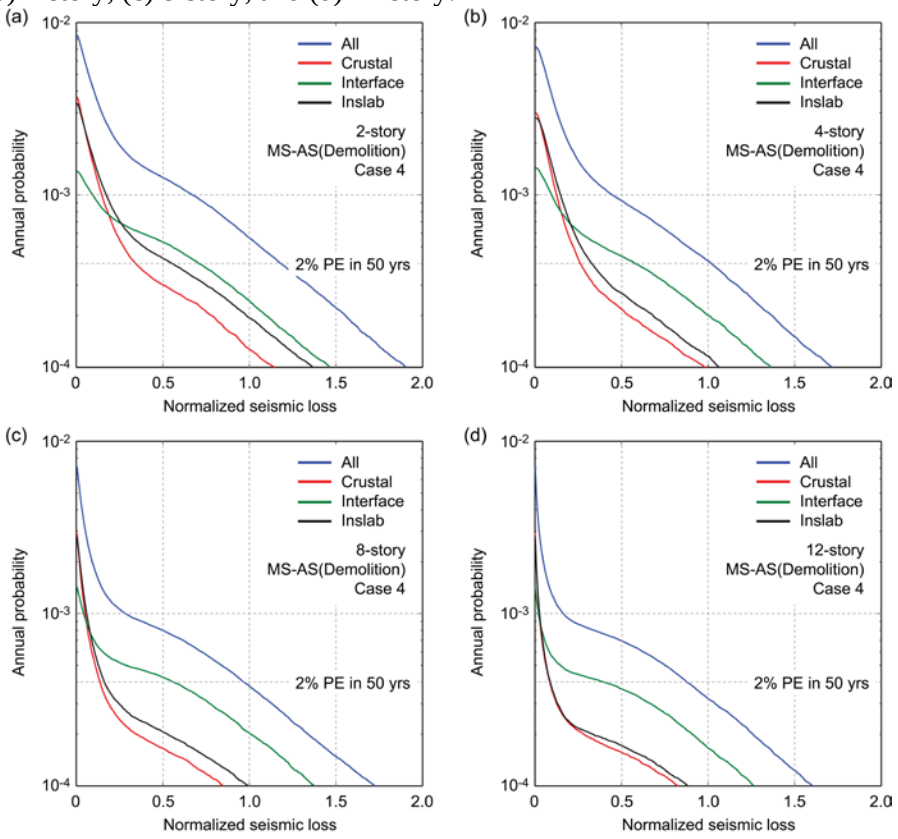

Figure 18. Seismic loss curves for MS-AS sequences and earthquake types (Case 4): (a) 2-story, (b) 4-story, (c) 8-story, and (d) 12-story.

The results confirm that the demolition limit state parameters and uncertainties of collapse fragility, non-collapse *EDP* prediction models, and *EDP-DV* functions are important. The

overall effects of major aftershocks on the estimated seismic loss are minor in comparison with other major factors for the 8- and 12-story buildings. However, large aftershocks can be major and imminent threat in post-disaster environments where structures are damaged by a mainshock and their capacities are reduced significantly (Maffei et al. 2008; Tesfamariam et al. 2015).

Table 3: Summary of normalized seismic loss at the annual exceedance probability of 4×10^{-4} (2% PE in 50 years) for four analysis cases.

Building height	Analysis type	Normalized seismic loss at annual exceedance probability of 4×10^{-4} (2% PE in 50 years)			
		Case 1	Case 2	Case 3	Case 4
2-story (Replacement cost: $6.125 million)	MS (Demolition)	0.971	0.895	1.127	1.057
	MS (No demolition)	0.880	0.891	1.054	1.047
	MS-AS (Demolition)	1.089	1.023	1.265	1.184
	MS-AS (No demolition)	1.015	1.023	1.187	1.184
4-story (Replacement cost: $12.6 million)	MS (Demolition)	0.984	0.858	1.096	0.996
	MS (No demolition)	0.799	0.809	0.939	0.946
	MS-AS (Demolition)	1.011	0.884	1.115	1.021
	MS-AS (No demolition)	0.797	0.796	0.935	0.949
8-story (Replacement cost: $19.93 million)	MS (Demolition)	0.826	0.785	0.965	0.933
	MS (No demolition)	0.783	0.800	0.920	0.895
	MS-AS (Demolition)	0.857	0.807	0.996	0.970
	MS-AS (No demolition)	0.807	0.802	0.939	0.949
12-story (Replacement cost: $29.03 million)	MS (Demolition)	0.796	0.712	0.918	0.887
	MS (No demolition)	0.685	0.652	0.838	0.878
	MS-AS (Demolition)	0.818	0.740	0.938	0.878
	MS-AS (No demolition)	0.713	0.723	0.863	0.878

The results show in Figures 17 and 18 can be used to compute the annual expected loss, and quantify contribution of the three earthquake types on the loss assessment (e.g. Goda and Tesfamariam 2016). Importantly, the detailed insights that can be obtained from disaggregated seismic loss curves based on earthquake types are particularly useful in deciding effective structural risk mitigation devices (e.g. dampers and isolation) for different buildings.

CONCLUSIONS

This study developed a comprehensive probabilistic seismic loss estimation methodology that accounts for main sources of uncertainty related to hazard, vulnerability, and loss. It considers not only mainshock hazards but also threat posed by major aftershocks and evaluates multi-variate damage accumulation process and failure modes (i.e. collapse, demolition, and non-collapse damage) quantitatively. The developed model was applied to 2-, 4-, 8-, and 12-story non-ductile RC buildings located in Victoria, BC, Canada, where seismic hazard

characteristics are contributed by shallow crustal, deep inslab, and mega-thrust Cascadia subduction earthquakes. Finite-element models that take into account key hysteretic characteristics of non-ductile RC frames were adopted. To reflect realistic and relevant ground motion information for Victoria, a new strong motion database for Japanese earthquakes was compiled and integrated into the existing database for MS-AS sequences. The database includes records from the 2011 Tohoku earthquake, which may be regarded as the closest surrogate to the possible M_w9 Cascadia subduction earthquake. A suitable set of input ground motion records was selected using the multiple CMS method based on detailed seismic hazard results. Seismic vulnerability of the RC frames was characterized through rigorous IDA and joint probabilistic modeling of multiple *EDP* variables. The seismic loss estimation adopted a story-based damage-loss methodology. From the parametric study, the following observations can be drawn:

- The earthquake event types have noticeable effects on the IDA results. For both MaxISDR and ResISDR, the IDA curves for interface events are severer than those for the crustal and inslab events.
- For the 2- and 4-story buildings, the collapse potential due to the interface events is greater than that due to the inslab and crustal events. Similarly, for the 8- and 12-story buildings, the collapse potential for the interface events is greater up to $IM = 0.4g$, and beyond this point, the collapse risk for the inslab events is higher.
- For all building heights, with increasing *IM* the normalized loss ratio increases for collapse damage, and decreases for non-collapse damage and demolition damage.
- The aftershocks have no appreciable effects on the 4-, 8-, and 12-story buildings in terms of seismic loss. However, for the 2-story building, the aftershocks showed marked increase in the seismic loss.
- For the 2- and 4-story building heights, the consideration of the demolition failure modes increases the seismic loss noticeably.
- With increasing building heights, 2- to 12-story, the difference in the loss associated with crustal and in-slab events diminishes. For the 12-story building, the difference is negligible.
- At annual probability of $10^{-2} – 10^{-3}$, crustal and in-slab events with $M_w6.5$ to $M_w7.5$ contributed the most to the loss as these events occur more frequently. At rarer annual

probability of 10^{-3} – 10^{-4}, the Cascadia event having M_w8.5 to M_w9.0 is predominant and contributed the most to the loss.

The non-code conforming RC buildings considered in this study are prone brittle, shear type failure. However, the OpenSees finite element model used in this study did not account for the potential shear failure. This study should further be extended to quantify the effect of shear modelling on the overall loss assessment.

ACKNOWLEDGEMENTS

Ground motion data for Japanese earthquakes and worldwide crustal earthquakes were obtained from the K-NET/KiK-net/SK-net databases at http://www.kyoshin.bosai.go.jp/ and http://www.sknet.eri.u-tokyo.ac.jp/, and the PEER-NGA database at http://peer.berkeley.edu/nga/index.html, respectively. This work was supported by the Natural Science Engineering Research Council Canada (RGPIN-2014-05013) to the first author and the Engineering and Physical Sciences Research Council (EP/M001067/1) to the second author.

REFERENCES

AIR Worldwide, 2013. *Study of Impact and the Insurance and Economic Cost of a Major Earthquake in British Columbia and Ontario/Québec*. Insurance Bureau of Canada, Toronto, Canada, 345 p.

Atkinson, G.M., and Goda, K., 2011. Effects of seismicity models and new ground motion prediction equations on seismic hazard assessment for four Canadian cities, *Bulletin of the Seismological Society of America* **101**, 176-189.

Baker, J.W., 2011. The conditional mean spectrum: a tool for ground motion selection, *Journal of Structural Engineering* **137**, 322-331.

Cornell, C.A., and Krawinkler, H., 2000. "Progress and challenges in seismic performance assessment," PEER Center News **3**(2). http://peer.berkeley.edu/news/2000spring/performance.html.

Ebrahimian, H., Jalayer, F., Asprone, D., Lombardi, A. M., Marzocchi, W., Prota, A., and Manfredi, G., 2014. A performance‐based framework for adaptive seismic aftershock risk assessment. *Earthquake Engineering & Structural Dynamics* **43**(14), 2179-2197.

Goda, K., and Taylor, C.A., 2012. Effects of aftershocks on peak ductility demand due to strong ground motion records from shallow crustal earthquakes, *Earthquake Engineering & Structural Dynamics* **41**, 2311-2330.

Goda, K., and Tesfamariam, S., 2015. Multi-variate seismic demand modelling using Copulas: Application to non-ductile reinforced concrete frame in Victoria, Canada, *Structural Safety* **56**, 39-51.

Goda, K., and Tesfamariam, S., 2016. Seismic risk management of existing reinforced concrete buildings in the Cascadia subduction zone, *ASCE Natural Hazard Review* doi: 10.1061/(ASCE)NH.1527-6996.0000206.

Goda, K., Atkinson, G.M., and Hong, H.P., 2011. Seismic loss estimation of wood-frame houses in south-western British Columbia, *Structural Safety* **33**, 123-135.

Goda, K., Kiyota, T., Mohan Pokhrel, R., Chiaro, G., Katagiri, T., Sharma, K. and Wilkinson, 2015. The 2015 Gorkha Nepal earthquake: insights from earthquake damage survey, *Frontiers in Built Environment* **1**,(8), http://dx.doi.org/10.3389/fbuil.2015.00008.

Goda, K., Wenzel, F., and De Risi, R., 2015. Empirical assessment of non-linear seismic demand of mainshock–aftershock ground-motion sequences for Japanese earthquakes, *Frontiers in Built Environment* **1**, doi:10.3389/fbuil.2015.00006.

Goldfinger, C., Grijalva, K., Bürgmann, R., Morey, A.E., Johnson, J.E., Nelson, C.H., Gutiérrez-Pastor, J., Ericsson, A., Karabanov, E., Chaytor, J.D., Patton, J., and Gràcia, E., 2008. Late Holocene rupture of the northern San Andreas fault and possible stress linkage to the Cascadia subduction zone, *Bulletin of the Seismological Society of America* **98**, 861-889.

Haselton, C.B., Liel, A.B., Lange, S.T., and Deierlein, G.G., 2008. *Beam-column Element Model Calibrated for Predicting Flexural Response Leading to Global Collapse of RC Frame Buildings.* PEER Report 2007/03, PEER Center, University of California, Berkeley, Berkeley, CA.

ICBO 1967. *Uniform Building Code*. International Conference of Building Officials, Pasadena, CA.

Koduru, S.D. and Haukaas, T., 2010. Probabilistic seismic loss assessment of a Vancouver high-rise building, *ASCE Journal of Structural Engineering*, **136**(3), 235-245.

Liel, A.B., and Deierlein, G.G., 2008. *Assessing the Collapse Risk of California's Existing Reinforced Concrete Frame Structures: Metrics for Seismic Safety Decisions*, Technical Report No. 166, John A. Blume Center Earthquake Engineering Center, Stanford, CA.

Luco, N., and Bazzurro, P., 2007. Does amplitude scaling of ground motion records result in biased nonlinear structural drift responses?, *Earthquake Engineering & Structural Dynamics* **36**, 1813-1835.

Maffei, J., Telleen, K., and Nakayama, Y., 2008. Probability-based seismic assessment of buildings, considering post-earthquake safety, *Earthquake Spectra* **24**, 667-699.

Mahsuli, M. and Haukaas, T., 2013. Seismic risk analysis with reliability methods, Part II: Analysis, *Structural Safety*, **42**(1), 63-74.

McNeil, A.J., Frey, R., and Embrechts, P., 2005. *Quantitative Risk Management: Concepts, Techniques and Tools*, Princeton University Press, Princeton, NJ.

Onur, T., Ventura, C.E., and Finn, W.D.L., 2005. Regional seismic risk in British Columbia - damage and loss distribution in Victoria and Vancouver. *Canadian Journal of Civil Engineering* **32**, 361-371.

Raghunandan, M. Liel, A.B. and Luco, N., 2015. Collapse risk of buildings in the Pacific Northwest region due to subduction earthquakes, *Earthquake Spectra* **31**(4), 2087-2115.

Ramirez, C.M., and Miranda, E., 2009. *Building-specific Loss Estimation Methods & Tools for Simplified Performance-based Earthquake Engineering*, Technical Report No. 171, John A. Blume Center Earthquake Engineering Center, Stanford, CA.

Ruiz-García, J., and Miranda, E., 2006. Residual displacement ratios for assessment of existing structures, *Earthquake Engineering & Structural Dynamics* **35**, 315-336.

Salami, M.R., and Goda, K., 2014. Seismic loss estimation of residential wood-frame buildings in south-western British Columbia considering mainshock-aftershock sequences, *Journal of Performance of Constructed Facilities* **28**, A4014002.

Tesfamariam, S., and Goda, K., 2015. Loss estimation for non-ductile reinforced concrete building in Victoria, British Columbia, Canada: effects of mega-thrust M_w9-class subduction earthquakes and aftershocks, *Earthquake Engineering & Structural Dynamics*, doi: 10.1002/eqe.2585.

Tesfamariam, S., Goda, K. and Mondal, G., 2015. Seismic vulnerability of RC frame with unreinforced masonry infill due to mainshock-aftershock earthquake sequences, *Earthquake Spectra* **31**, 1427-1449.

Vamvatsikos, D., and Cornell, C.A., 2002. Incremental dynamic analysis, *Earthquake Engineering & Structural Dynamics* **31**, 491-514.